Available online at www.sciencedirect.com

ScienceDirect

Solar Energy 118 (2015) 533–546

SOLAR ENERGY

www.elsevier.com/locate/solener

Electrical-thermal analysis of III–V triple-junction solar cells under variable spectra and ambient temperatures

Marios Theristis *, Tadhg S. O'Donovan

Institute of Mechanical, Process and Energy Engineering, School of Engineering and Physical Sciences, Heriot-Watt University, Edinburgh EH14 4AS, United Kingdom

Received 6 August 2014; received in revised form 4 May 2015; accepted 3 June 2015
Available online 23 June 2015

Communicated by: Associate Editor Takhir M. Razykov

Abstract

The influence of the incident spectral irradiance on the electrical and thermal behaviour of triple-junction solar cells has been investigated. A spectral dependent electrical model has been developed to calculate the electric characteristics and quantify the heat power of a multijunction solar cell. A three-dimensional finite element analysis is also used to predict the solar cell's operating temperature and cooling requirements for a range of ambient temperatures. The combination of these models improves the prediction accuracy of the electrical and thermal behaviour of triple-junction solar cells. The convective heat transfer coefficient between the back-plate and ambient air was found to be the significant parameter in achieving high electrical efficiency. These data are important for the electrical and thermal optimisation of concentrating photovoltaic systems under real conditions. The objective of this work is to quantify the temperature and cooling requirements of multijunction solar cells under variable solar spectra and ambient temperatures. It is shown that single cell configurations with a solar cell area of 1 cm^2 can be cooled passively for concentration ratios of up to 500× with a heat sink thermal resistance below 1.63 K/W, however for high ambient temperatures (greater than 40 °C), a thermal resistance less than 1.4 K/W is needed to keep the solar cell operating within safe operating conditions.

Keywords: Concentrating photovoltaic; Triple-junction solar cells; Cooling requirements; Electrical and thermal modelling

1. Introduction

Multijunction (MJ) solar cells are made of III–V compound semiconductors and are used in space and terrestrial applications. Currently the state-of-art solar cell on the market is the lattice matched triple-junction (3J) solar cell made of GaInP/GaInAs/Ge subcells (Guter et al., 2009; Helmers et al., 2013). These subcells, are monolithically connected in series in a specific way to absorb a larger proportion of the solar spectrum and thus, to achieve higher conversion efficiencies. To date, the highest recorded efficiency for a 3J solar cell is 44.4% and 46% for 4J (NREL, 2015). Such solar cells can be economically viable if sunlight is concentrated by a factor greater than 300× (Cotal and Frost, 2010; Kinsey et al., 2008; Verlinden et al., 2006).

High concentrations result in high heat flux on the solar cell's surface and a rapid increase in the cell's temperature. High temperatures reduce the electrical conversion efficiency because of the temperature dependence of the open-circuit voltage (V_{oc}) and the maximum power voltage (V_{mp}) (Cotal and Sherif, 2006). It has been shown that under 500× concentration and without any cooling

* Corresponding author.
E-mail address: mt208@hw.ac.uk (M. Theristis).

http://dx.doi.org/10.1016/j.solener.2015.06.003
0038-092X/

Nomenclature

A	area (m^2)
AM	air mass (–)
c	speed of light in vacuum (m/s)
C_p	heat capacity (J/(kg K))
CR	concentration ratio (–)
DNI	direct normal irradiance (W/m^2)
EQE	external quantum efficiency (–)
E_g	energy band-gap (eV)
$G(\lambda)$	spectral DNI ($W/m^2/nm$)
h	Planck's constant (J s)
h_{conv}	conv. heat transfer coeff. ($W/(m^2K)$)
I	current (A)
I_{sc}	short-circuit current (A)
I_0	dark saturation current (A)
J	current density (A/m^2)
J_{sc}	short-circuit current density (A/m^2)
J_0	dark saturation current density (A/m^2)
k	thermal conductivity (W/(m K))
k_B	Boltzmann constant (eV/K)
K_c	R_s intensity coefficient (–)
n	diode ideality factor (–)
P_{in}	incident power (W)
P_m	maximum power output (W)
q	elementary charge (C)
q_{heat}	heat power (W)
q''	heat flux rate (W/m^2)
q'''_{heat}	heat generation (W/m^3)
R_s	series resistance (Ω)
R_{sh}	shunt resistance (Ω)
R_{S0}	R_s at low intensity (Ω)
$R_{s\infty}$	R_s at high flux (mΩ)
R_{th}	thermal resistance (K/W)
s	number of cycle iterations (–)
T_{amb}	ambient temperature (°C)
T_c	solar cell's temperature (°C)
V	voltage (V)
V_{mp}	voltage at maximum power (V)
V_{oc}	open-circuit voltage (V)
X	ratio of top to middle J_{sc} (–)
z	zenith angle (°)

Greek letters

α	material dependent constant (eV/K)
β	material dependent constant (K)
γ	constant (–)
ΔT	temperature difference (°C)
ε	emissivity (–)
η_{cell}	electrical efficiency (–)
η_{opt}	optical efficiency (–)
κ	constant ($A/(cm^2K^4)$)
λ	wavelength (nm)
ρ	density (kg/m^3)
σ	Stefan-Boltzmann constant ($W/(m^2K^4)$)

Abbreviations

Al_2O_3	Aluminium Oxide or Alumina
CCA	Concentrator Cell Assembly
CPV	Concentrating Photovoltaic
CSTC	Concentrator Standard Test Conditions
DBC	Direct Bonded Copper
EM	Electrical Model
FEA	Finite Element Analysis
FETM	Finite Element Thermal Model
GaInAs	Gallium Indium Arsenide
GaInP	Gallium Indium Phosphide
Ge	Germanium
GMRES	Generalised Minimal RESidual method
HCPV	High Concentrating Photovoltaic
IR	Infrared
MJ	Multijunction
MPP	Maximum Power Point
RMSE	Root Mean Square Error
SMARTS2	Simple Model of the Atmospheric Radiative Transfer of Sunshine, version 2
UV	Ultraviolet
3J	Triple-junction

arrangements, the solar cell can exceed 1000 °C (Araki et al., 2002; Cotal and Frost, 2010; Kuo et al., 2009; Min et al., 2009; Nishioka et al., 2006; Ye et al., 2009). This emphasises the need for appropriate cooling technology to decrease the temperature to within safe operation limits and to avoid suboptimal performance and risk of system failure.

The recommended operating temperature varies for different manufacturers; Spectrolab Inc. suggests a maximum operating cell temperature of 100 °C (Spectrolab, 2009b), Azurspace GmbH 110 °C for their latest product 3C42A (Azurspace, 2014) and 150 °C for the old product 3C40A (Azurspace, 2010) while Sharp data are given for up to 120 °C (Segev et al., 2012). Reliability analysis on 3J solar cells have shown that, at operating conditions of 820× and 80 °C, the warranty time was found to be 113 years; at 100 °C however, the warranty time was reduced to 7 years (Espinet-González et al., 2014). It is also worth noting that, in high temperatures (over 120 °C, 1×), the voltage output of the low energy band-gap germanium subcell decreases to almost zero (Helmers et al., 2013; Nishioka et al., 2005). Therefore, to avoid long term degradation problems and

also the risk of destroying the connections (melting), the concentrator cell assembly (CCA) should not operate in excess of 100 °C.

MJ solar cells are usually characterised in laboratory facilities under Concentrator Standard Test Conditions (CSTC). These conditions correspond to cell temperature $T_c = 25$ °C, air mass 1.5 direct (AM1.5D) and Direct Normal Irradiance $DNI = 1$ kW/m^2, although in the field, the atmospheric conditions can vary significantly (Kinsey, 2010). Due to the fact that the subcells of the 3J solar cell are monolithically connected and also because of their sensitivity to the spectral variations and intensity of sunlight, the prediction of the electrical and thermal behaviour is still challenging (Steiner et al., 2012). There also exists a limitation relating to the in-series connection of such solar cells; a mismatch in the current produced by each subcell will limit the overall output to the lower value; this, in turn will result in greater heat production within the cell. Therefore, by applying a simple *DNI* value as an input in thermal models may give inaccurate results. It is important therefore, to develop smart algorithms, models or methods to realistically determine the electrical performance of the cell to accurately determine the thermal characteristics, temperature and cooling requirements of the system.

Concentrating photovoltaic (CPV) thermal numerical models and experimental designs have been thoroughly discussed in literature using passive (Araki et al., 2002; Chou et al., 2012; Kuo et al., 2009; Natarajan et al., 2011; Wang et al., 2013) and active (Al-Amri and Mallick, 2013; Kribus et al., 2006; Royne and Dey, 2007; Zhu et al., 2011) cooling techniques. According to Royne et al. (2005), who presented an extensive review on different cooling techniques, passive cooling can be sufficient for single cell geometries and solar flux up to 1000 suns where a "large area" is available below the cell for a heat sink. For densely packed cells and concentration ratios (*CR*) higher than 150 suns, active cooling is necessary (Royne et al., 2005). It was also concluded that the thermal resistance (R_{th}) of the cooling system must be less than 10^{-4} m^{2}K/W for concentration levels above 150×. However, the spectral effects on electrical efficiency and hence, the temperature are not included in the aforementioned thermal models.

In addition, the prediction of solar cell's temperature is very important for the electrical characterisation of CPV modules. Rodrigo et al. (2014) reviewed various methods for the calculation of the cell temperature in High Concentrator PV (HCPV) modules. The methods were categorised based on: (1) heat sink temperature, (2) electrical parameters and (3) atmospheric parameters. The first two categories are based on direct measurements of CPV modules in indoor or outdoor experimental setups and presented the highest degree of accuracy (Root Mean Square Error (RMSE) 1.7–2.5 K). Most of the methods reviewed by Rodrigo et al. (2014) calculate the cell temperature at open-circuit conditions. Methods that predict the cell temperature at maximum power point (MPP) operation offer a more realistic approach since they include the electrical energy generation of the solar cells (i.e. real operating conditions); Yandt et al. (2012) described a method predicting the cell temperature at MPP based on electrical parameters and Fernández et al. (2014b) based on heat sink temperature with absolute RMSE 0.55–1.44 K. Fernández et al. (2014a) also proposed an artificial neural network model to estimate the cell temperature based on atmospheric parameters and an open-circuit voltage model based on electrical parameters (Fernandez et al., 2013a) offering good accuracy (RMSE 3.2 K and 2.5 K respectively (Rodrigo et al., 2014)). The main disadvantage of the aforementioned methods is that an experimental setup is required to obtain the parameters used for the cell temperature calculation.

Despite the fact that several electrical models and experimental procedures for MJ solar cells have been described thoroughly in literature (Ben Or and Appelbaum, 2013; Dominguez et al., 2010; Fernández et al., 2013; Fernandez et al., 2013b; Kinsey and Edmondson, 2009; Kinsey et al., 2008; Rodrigo et al., 2013; Segev et al., 2012; Siefer and Bett, 2014) which included the spectrum and irradiance dependence, the challenge to develop an integrated thermal-electrical model which predicts the cell temperature and includes the cooling needs is still unsolved. This study builds on a methodology (Theristis and O'Donovan, 2014) which considered a constant spectral response at 25 °C and AM1.5D. The current methodology combines three models; the solar spectral irradiance is generated by the NREL Simple Model of the Atmospheric Radiative Transfer of Sunshine, version 2 (SMARTS2) (Gueymard, 1995, 2001; Gueymard et al., 2002), an electrical model (EM) uses a single diode model to simulate the electrical characteristics and heat power of a 3J solar cell at MPP (i.e. connected to an inverter) and a finite element analysis thermal model (FETM) that uses the heat power as an input from the electrical model in order to predict the temperature and the cooling requirements as a function of ambient temperature.

2. Theory

2.1. Electrical model (EM)

The single diode model was used to model the electrical characteristics of a 3J solar cell. According to Segev et al. (2012), the one-diode equivalent circuit model is adequate to describe a 3J solar cell in practical applications. Each junction of the solar cell can be represented by an equivalent circuit model and therefore, by connecting them in series, the one diode equivalent circuit model for a 3J solar cell can be obtained (Fig. 1). This model differs from the two diodes in the number of diodes that describe the saturation current. In the single diode model, the diode represents recombination in both the depletion and quasi-neutral regions (Segev et al., 2012).

If the shunt resistances ($R_{sh,i}$) are sufficiently large to be neglected, the current density–voltage (*J*–*V*) relationship is given by

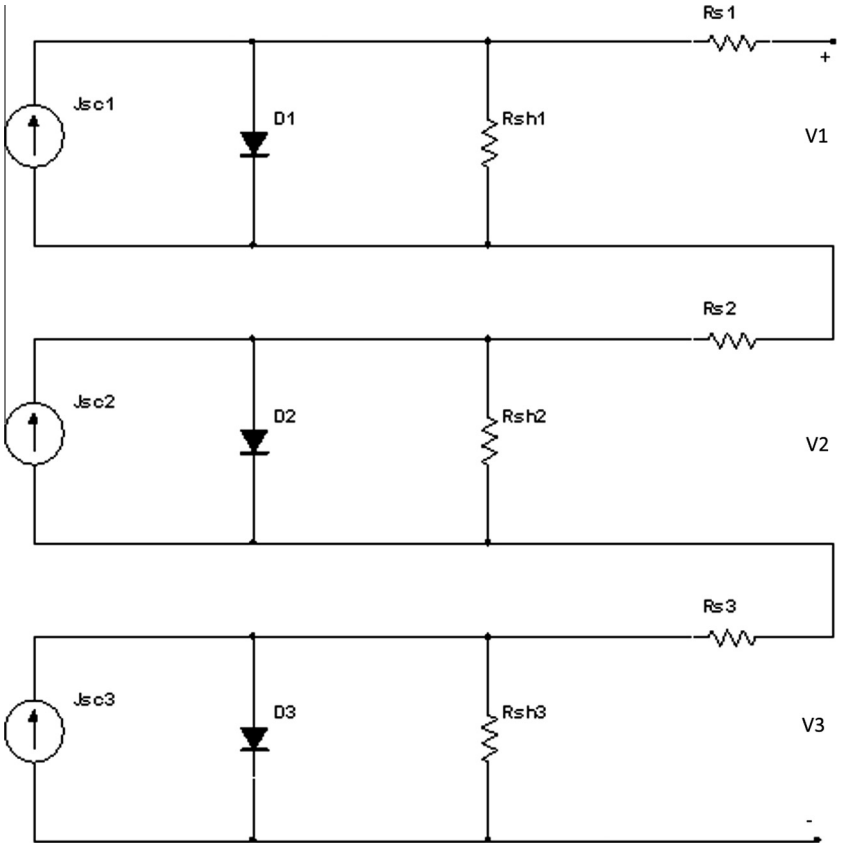

Fig. 1. One-diode equivalent circuit 3 J cell model (Segev et al., 2012).

$$J_i(V) = J_{0,i}(T_c) \cdot \left(e^{\frac{q(V_i - J_i \cdot A \cdot R_s)}{n_i \cdot k_B \cdot T_c}} - 1\right) - J_{SC,i}(T_c), \quad (1)$$

where i is an index for each subcell (1 for top, 2 for middle and 3 for bottom), J_0 the dark saturation current density, q the elementary charge, V the voltage, J is the current density, A the area, R_s the series resistance, n the diode ideality factor, k_B the Boltzmann constant and J_{SC} is the short-circuit current density. The dark saturation current density is strongly affected by temperature and is described as

$$J_{0,i}(T_c) = k_i \cdot T_c^{(3+\gamma_i/2)} e^{(-E_{g,i}(T_c)/n_i \cdot k_B \cdot T_c)}, \quad (2)$$

where k and γ are constants. The energy band-gap E_g, decreases with increasing temperature and is given by the Varshni relation (Varshni, 1967):

$$E_{g,i}(T_c) = E_{g,i}(0) - \frac{\alpha_i T_c^2}{T_c + \beta_i}, \quad (3)$$

where $E_{g,i}(0)$ is the energy band-gap of i subcell at 0 K and α, β are material dependent constants. The short-circuit current density distribution for each subcell as a function of temperature is calculated using Eq. (4):

$$J_{sc,i}(T_c) = \int_{\lambda_{i,\min}}^{\lambda_{i,\max}} \frac{q \cdot \lambda \cdot EQE_i(\lambda, T_c) \cdot \eta_{opt}(\lambda) \cdot CR \cdot G(\lambda)}{h \cdot c} \cdot d\lambda, \quad (4)$$

where $\lambda_{i,\min}$ and $\lambda_{i,\max}$ correspond to the wavelength range of each subcell, λ is the wavelength of the incident photons, EQE_i is the External Quantum Efficiency, η_{opt} the optical efficiency, CR is the concentration ratio, $G(\lambda)$ is the spectral DNI, h is Planck's constant and c the speed of light in a vacuum. EQE is defined as the ratio of the number of carriers collected by the cell to the number of incident photons.

The total current density output due to the series connection is given by the minimum current density of the three subcells;

$$J = \min(J_1, J_2, J_3). \quad (5)$$

Solving Eq. (1) for $J_i = 0$, the open-circuit voltage for each subcell is obtained:

$$V_{oc,i} = \frac{n_i \cdot k_B \cdot T_c}{q} \ln\left(\frac{J_{sc,i}(T_c)}{J_{0,i}(T_c)} + 1\right). \quad (6)$$

The voltage in each junction can be also calculated by rearranging Eq. (1):

$$V_i = \frac{n_i \cdot k_B \cdot T_c}{q} \ln\left(\frac{J_{SC,i}(T_c) - J_i}{J_{0,i}(T_c)} + 1\right) - J_i \cdot A \cdot R_{s,i}. \quad (7)$$

The total voltage output is the sum of the voltage in each junction, therefore:

$$V = \sum_{i=1}^{3} V_i,$$
$$V = \frac{k_B \cdot T_c}{q}\left[\sum_{i=1}^{3} n_i \ln\left(\frac{J_{SC,i}(T_c) - J}{J_{0,i}(T_c)} + 1\right)\right] - J \cdot A \cdot R_s. \quad (8)$$

The solar cell's efficiency is defined as the proportion of the maximum power output of the cell to the *DNI* which is incident on the cell:

$$\eta_{cell} = \frac{P_{out}}{P_{in}} = \frac{P_m}{\int_{280}^{4000} CR \cdot A \cdot \lambda \cdot G(\lambda) \cdot \eta_{opt}(\lambda) \cdot d\lambda}. \quad (9)$$

Therefore, the heat power produced on the cell is

$$q_{heat} = P_{in} \cdot (1 - \eta_{cell}). \quad (10)$$

2.2. Thermal model (FETM)

An analytical FETM has been developed to predict the thermal behaviour of 3J solar cells. The multijunction solar cell is attached to a Direct Bonded Copper (DBC) substrate for heat dissipation and electrical insulation. The heat is transferred by conduction between the solid layers of the receiver. Some heat is lost to the environment, due to natural convection and surface to ambient radiation from all free surfaces.

In the case of a passively or actively cooled receiver, the heat is transferred by conduction between the solid layers of the receiver and the steady state equation is given by the Fourier's law of heat conduction:

$$q''_{cond} = -k\nabla T, \quad (11)$$

where q'' is the heat flux rate (W/m^2), k the heat conductivity and ∇ is the three-dimensional operand. The solar flux that is transformed to heat must be dissipated from the bottom substrate or cooling system to the environment or harnessed for use in another application. The heat which is dissipated either by natural or forced convection is described by

$$q''_{n/f,conv} = h_{n/f} \cdot \Delta T, \quad (12)$$

where h is the heat transfer coefficient (natural or forced) and ΔT the temperature difference between the cell and the ambient air or ultimate heat sink. The heat, which is lost to the environment, due to natural convection occurs on every surface that faces the ambient. COMSOL Multiphysics contains the correlations for each surface orientation (vertical, horizontal or inclined); these can be found in Incropera and DeWitt (1996). The heat loss due to radiation is given by:

$$q''_{rad} = \varepsilon \cdot \sigma \cdot (T^4 - T^4_{amb}), \quad (13)$$

where ε is the material's emissivity and σ the Stefan–Boltzmann constant. The heat transfer at solid interfaces is defined by the following heat equation to simulate the thermal behaviour:

$$q'''_{heat} = \rho \cdot C_p \frac{\partial T}{\partial t} - \nabla \cdot (k\nabla T), \quad (14)$$

where the first term disappears in steady state problems and q'''_{heat} is the heat source (W/m^3) which is calculated from the electrical model divided by the cell volume.

3. Methodology

The models described above are simulated based on the flowchart in Fig. 2. The solar spectrum is generated using the SMARTS2. Clear sky days are assumed and the zenith angle (z), and hence the air mass (AM) is considered to be the only variant that affects the direct spectral irradiance.

The simulations are conducted in steady state. The EM runs for a given CR, an initial T_c of 25 °C, AM1D $\leqslant AM \leqslant$ AM15D and the heat power is then introduced in the 3D FETM in COMSOL. Solar spectra ranging from AM1D to AM15D have been chosen as a rigorous test for this integrated model. They are not location specific; they are used to demonstrate the applicability of the model to a wide range of solar geometries. For 25 °C $\leqslant T_{amb} \leqslant$ 45 °C and 1200 W/(m^{2}K) $\leqslant h_{conv} \leqslant$ 1600 W/(m^{2}K) at the back surface of the CCA, the cell's temperature is predicted from the thermal model and is then imported to the electrical model. The procedure is repeated until a steady state is reached; i.e. $|T_c(s) - T_c(s+1)| \leqslant 0.002$ K, where s is the number of cycle iterations. Table 1 summarises the variable input parameters used for the simulation program, the range of each parameter, the model from which they are generated and the model that uses them as an input. The maximum convective heat transfer coefficient considered in this study is 1600 W/(m^{2}K), as this has been shown by Mudawar (2001) to be the maximum achievable under passive cooling conditions. Lower convective heat transfer coefficients are not reported as they were found to be insufficient to maintain the cell temperature below 100 °C.

4. Results & discussion

This section describes an application of the aforementioned methodology using the C1MJ CCA from Spectrolab. Literature based data from Kinsey and Edmondson (2009) and Segev et al. (2012) are used in the EM. The CR discussed in this section is for 500× unless otherwise stated.

4.1. SMARTS2

The generated direct spectral irradiance from SMARTS2 is shown in Fig. 3. For the sake of clarity some air mass values are not illustrated. The integration of the spectral irradiance at a specific air mass gives the irradiance intensity; the values are shown in Fig. 5 as a function of z. Other parameters were kept constant at the reference conditions of the standard ASTM G173-03 (Gueymard and Myers, 2010) (precipitable water 1.42 cm, rural aerosol

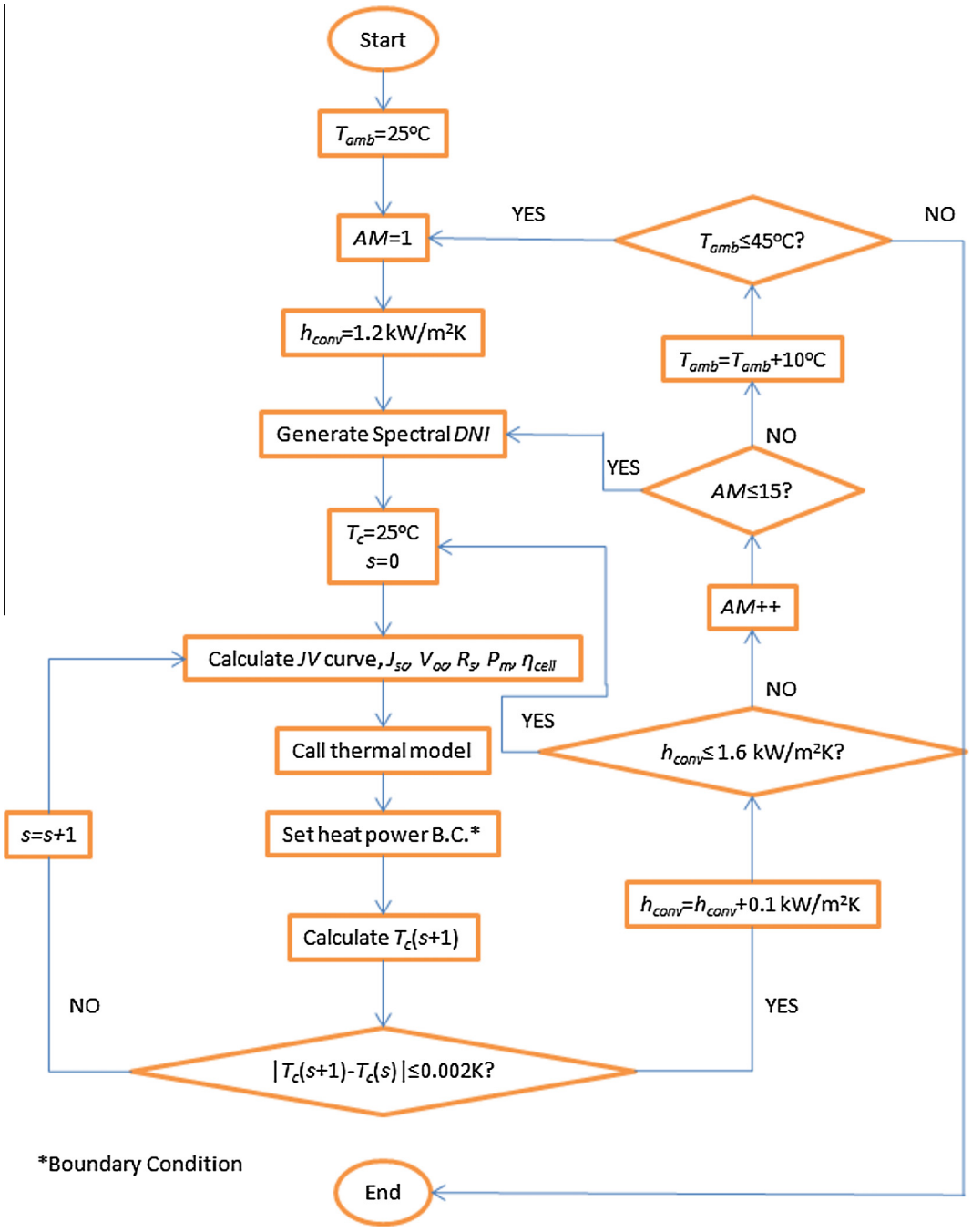

Fig. 2. Flowchart of simulation program.

Table 1
Model variables.

Variable input parameter	Range	Generated from	Used in
AM	1–15	SMARTS2	EM
h_{conv}	1.2–1.6 kW/(m^{2}K)		FETM
q_{heat}		EM	FETM
T_c		FETM	EM
T_{amb}	25–45 °C		FETM

model, turbidity value 0.084 specified as aerosol optical depth at 500 nm). Fig. 4 shows the percentage of ultraviolet (UV, 280–400 nm), visible (400–780 nm) and infrared (IR, >780 nm) light as a function of air mass. It can be seen that for $AM \geqslant$ AM3D the IR wavelengths have the highest proportion while the UV component is zero for $AM >$ AM7D.

4.2. Electrical model (EM)

The *EQE* of the Spectrolab C1 MJ multijunction solar cell, as characterised by Kinsey and Edmondson (2009) for a temperature range between 25 °C and 75 °C, was used

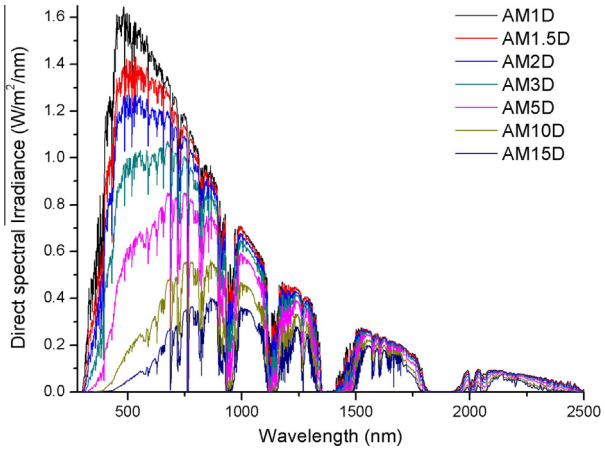

Fig. 3. Direct spectral irradiance generated by SMARTS2 for AM1D to AM15D. Some air mass values are not illustrated for clarity purposes.

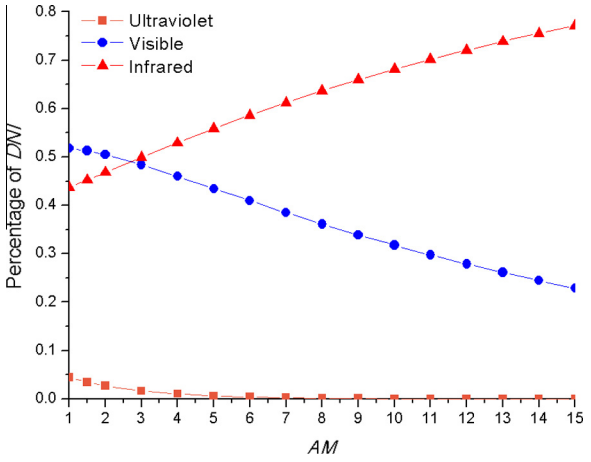

Fig. 4. Ultraviolet, visible and infrared light percentage of direct normal irradiance as a function of air mass.

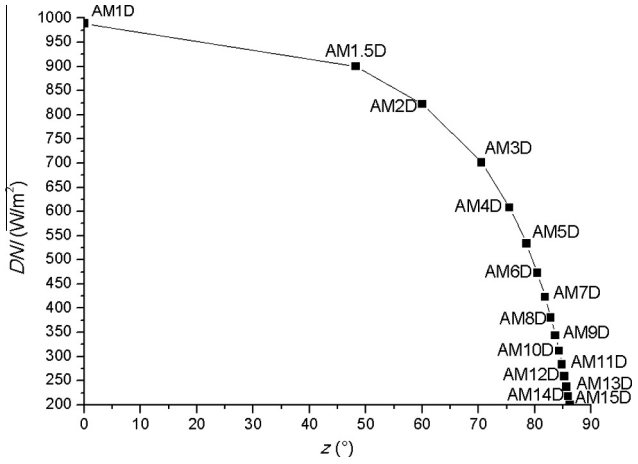

Fig. 5. Direct intensity versus zenith angle and air mass. Intensity values are calculated by integrating the solar spectral irradiance.

for this application. The bottom subcell was measured using a C1MJ subcell isotype.

The input parameters used for the electrical model are listed in Table 2. The cell area was taken as $A = 1\ \text{cm}^2$ and the optical efficiency $\eta_{opt} = 0.8$. The series resistance as a function of the incident power was calculated according to Spectrolab (2009a):

$$R_s = \frac{R_{S0}}{CR^{K_c}} + R_{s\infty}, \tag{15}$$

where $R_{S0} = 11\ \text{m}\Omega$ is the series resistance at low intensity, $R_{s\infty} = 40\ \Omega$ is the series resistance at high flux and $K_c = 1.75$ is a series resistance intensity coefficient. Table 3 shows the fitting parameters for the C1MJ single diode model which were adopted directly from Segev et al. (2012).

4.2.1. Short-circuit current density

From Eq. (4), the J_{sc} distribution for each subcell can be calculated. As mentioned above (see Section 2.1.), higher T_c decreases each subcell's band-gap causing the EQE to shift towards the longer wavelengths and therefore the J_{sc} follows the same behaviour ($J_{sc,3}$ is plotted separate for clarity, see Figs. 6 and 7). Figs. 8 and 9 show the effect of AM; higher air mass values show a significant drop in the short wavelength region (see also Figs. 3 and 4) and therefore the effect on higher band-gap subcells is higher than the low band-gap (germanium) subcell. This will be the case especially for $J_{sc,1}$ which decreases rapidly for $AM >$ AM2D acting as the current limiting subcell. Also considering that in the winter period, the AM will always be greater or equal to 2 at middle to high latitudes, the subcells will never be current matched (Faine et al., 1991). This has an impact on the electrical performance of the cell since the excess current will be transformed directly to heat. Moreover, by comparing Figs. 3 and 4 with Figs. 6–9, it is apparent that the germanium subcell will never limit the current output.

4.2.2. Total open-circuit voltage

The V_{oc} dependence on temperature under variable AM is plotted in Fig. 10. Increasing temperatures result to an increase in the J_0 which, in turn, decreases the V_{oc} (see also Eqs. 2, 3 and 6). The relative temperature coefficient range is between −0.16%/K for AM1D to −0.18%/K for AM15D. This shows that there is only a weak dependency of AM change on the V_{oc} temperature coefficient. By increasing the AM, the V_{oc} decreases by 0.48%/AM at 25 °C, 0.56%/AM at 45 °C, 0.61%/AM at 65 °C and 0.63%/AM at 75 °C. This reduction is due to the J_{sc} decrease.

Table 2
Inputs of electrical model.

Subcell	α (eV/K)	β (K)	E_g at 0 K (eV)
1	4.72×10^{-4}	269	1.86
2	5.39×10^{-4}	204.7	1.495
3	4.77×10^{-4}	235	0.756

Table 3
Fitting parameters for C1MJ single diode model adopted directly from Segev et al. (2012).

Subcell	κ (A/(cm^{2}K^4))	γ	n
1	1.833×10^{-8}	1.81	1.89
2	2.195×10^{-7}	1.86	1.59
3	1.9187×10^{-5}	1.44	1.43

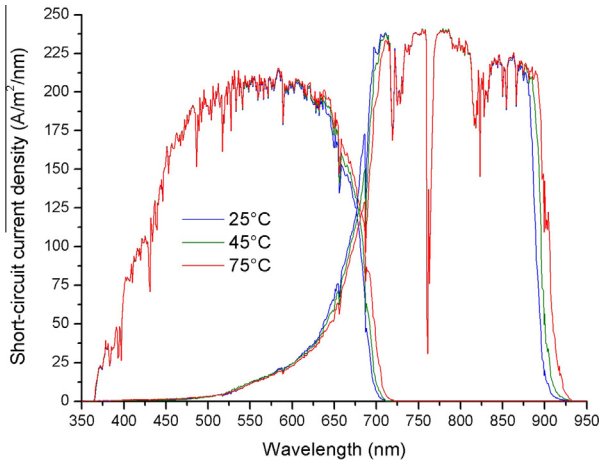

Fig. 6. Short-circuit current density distribution of top and middle subcell under 500× and AM1.5D as a function of temperature.

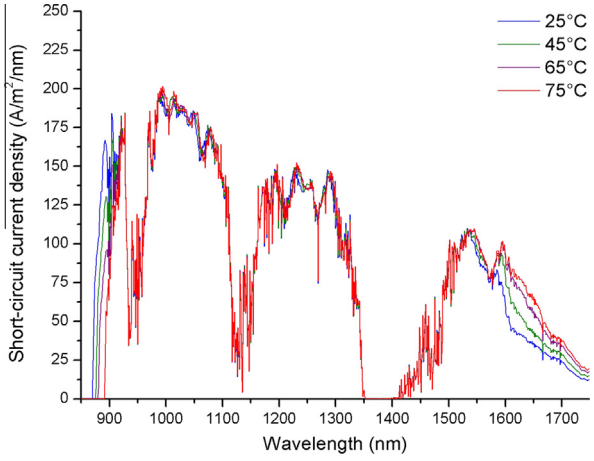

Fig. 7. Short-circuit current density distribution of bottom subcell under 500× and AM1.5D as a function of temperature.

4.2.3. Efficiency

Since the bottom subcell will never limit the current (as explained in Section 4.2.1.) the ratio of the top to the middle subcell's short-circuit current density ($X = J_{sc,1}/J_{sc,2}$) is used for comparison. Fig. 11 shows that the maximum efficiency is achieved when the top and middle subcells are current matched under any temperature. Also the middle subcell is the current limiting cell only for air mass values lower than AM1.5D while for all other air mass values the current limiting subcell is the top subcell. X is shown only for 25 °C for clarity purposes because it is very close to the short-circuit current ratio at higher temperatures

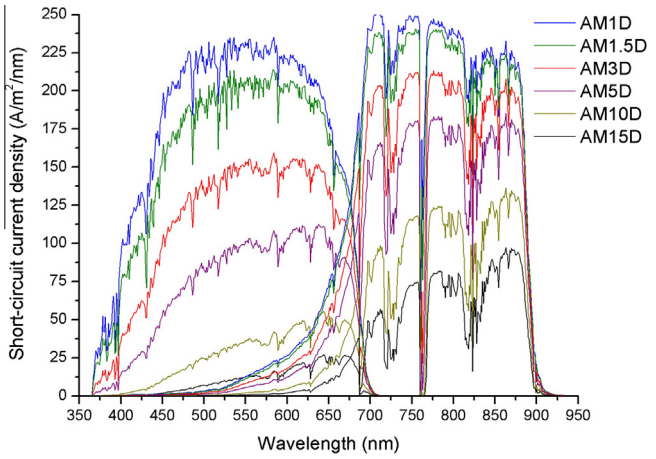

Fig. 8. Effect of AM on short-circuit current density distribution of top and middle subcell under 500× and $T_c = 25$ °C.

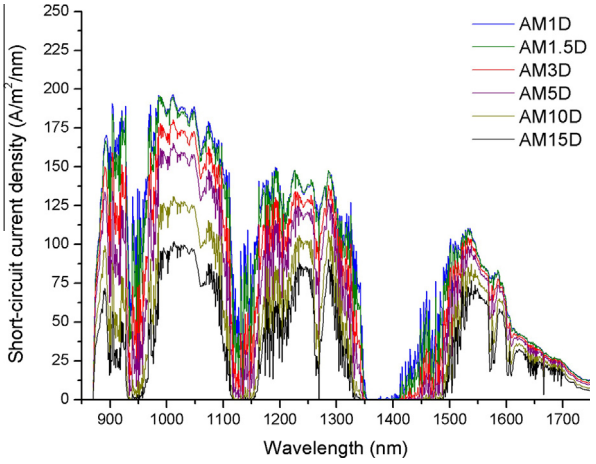

Fig. 9. Effect of AM on short-circuit current density distribution of bottom subcell under 500× and $T_c = 25$ °C.

(X at 75 °C is 0.58% higher for AM1D and 3% for AM15D).

4.2.4. Heat power

The analysis of the triple-junction solar cell's electrical output is important to quantify the heat power which is produced and needs to be dissipated by the cooling mechanism. In order to calculate the heat power over a range of air mass values and temperatures, Eq. (10) is used. The maximum heat power is found to be 25.5 W at AM1D and 75 °C (Fig. 12). Inset graph in Fig. 12 shows the air mass values of interest for the thermal model; thermal issues are not significant for $AM >$ AM2D, since any cooling mechanism which is designed to dissipate the heat at $AM \leqslant$ AM2D, will be adequate for any range of higher air mass values.

4.2.5. Current mismatch effect on heat power

The maximum heat power produced on the cell due to current mismatch is quantified using Eq. (16) (Rabady,

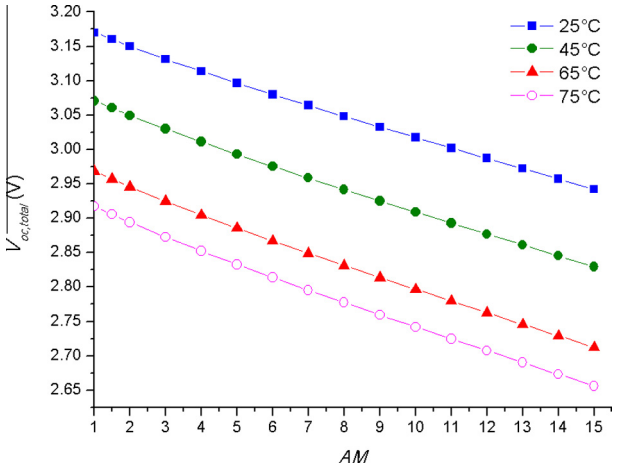

Fig. 10. C1MJ total open-circuit voltage at $CR = 500\times$ under variable air mass and cell temperature.

2014) and is shown graphically in Fig. 13. The minimum heat power due to current mismatch is found when the top and middle subcells generate the same current (i.e. under AM1.5D), however the increasing operating temperature shows a reduction of 13% which is due to the reduction of the E_g which in turn reduces the V_{oc}. For $AM >$ AM2D the heat increases sharply because a subcell limits the current until $AM >$ AM7D where the heat power is reduced mainly due to the decrease in the spectral irradiance intensity.

$$q_{heat,CM} \leqslant \sum_{1}^{3} |I_{sc,i} - I_{total}| \cdot V_{OC,i} \tag{16}$$

4.2.6. Validation of electrical model

For validation purposes, the electrical model was simulated for $CR = 555\times$, $\eta_{opt} = 1$ and was compared with measured data from Kinsey and Edmondson (2009). The C1MJ short-circuit current density values were adopted

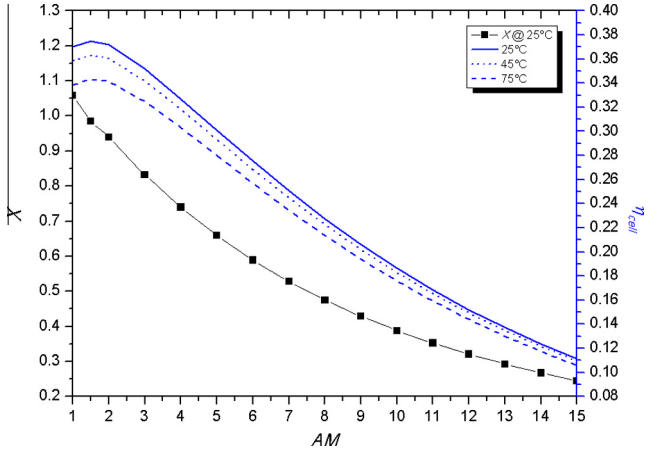

Fig. 11. Ratio of top to middle subcell's short-circuit current density, X at 25 °C (left black axis) and cell's efficiency (right blue axis) at $CR = 500\times$ over a range of air mass values and cell temperatures. (For interpretation of the references to colour in this figure legend, the reader is referred to the web version of this article.)

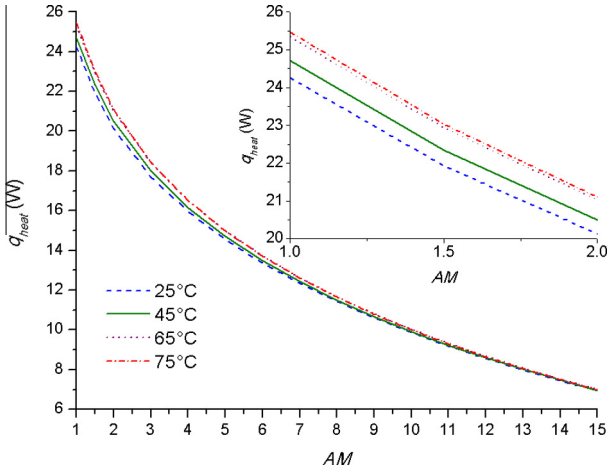

Fig. 12. Heat power at $CR = 500\times$ over a range of cell temperatures and air mass values; inset graph shows the air mass values of interest for the thermal model.

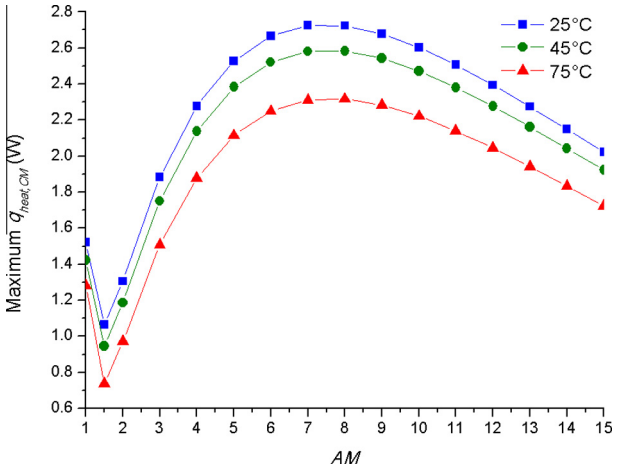

Fig. 13. Maximum heat power produced on the solar cell due to current mismatch for a range of air mass values and operating temperatures at $CR = 500\times$.

directly from Kinsey and Edmondson (2009) for the four measured temperatures. The RMS error for the efficiency was calculated according to:

$$RMSE = \sqrt{\frac{\sum_{i=1}^{m} \left(\eta_{cell,meas}(T_c) - \eta_{cell,calc}(T_c)\right)^2}{m}}, \tag{17}$$

where $\eta_{cell,meas}$ is the measured electrical efficiency at T_c from Kinsey and Edmondson (2009) and $\eta_{cell,calc}$ is the calculated electrical efficiency from the model. These are shown graphically in Fig. 14 for RMS error 0.25%.

4.3. Thermal model (FETM)

The calculated heat power from the electrical model was used as an input to the thermal model. The geometry and thermal boundary conditions of the C1MJ model are shown in Fig. 15 and Table 4. The 3J solar cell is modelled

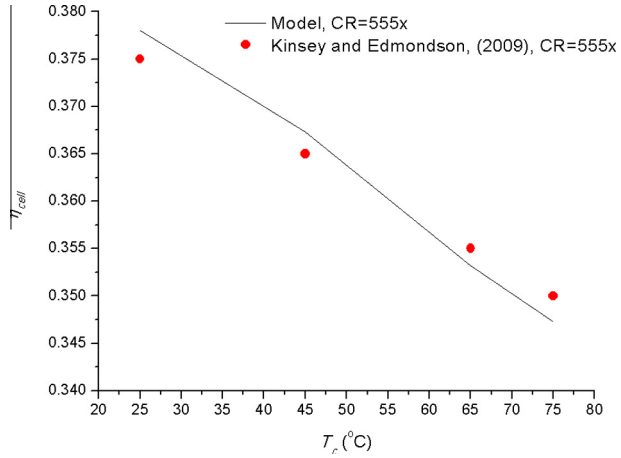

Fig. 14. C1MJ efficiency under variable cell temperature for AM1.5D, $CR = 555\times$, $\eta_{opt} = 1$ and comparison with published data, Kinsey and Edmondson (2009).

as one entity (Germanium cell) because the top and middle subcells are much thinner than the bottom and therefore they would not affect the thermal model. This statement is confirmed by Chou et al. (2012). The solar cell is attached on a DBC substrate which is made of copper/Al_2O_3 ceramic/copper. The electrical connections are made of silver. The cell is connected to a 12A Schottky diode which, for simplicity is not modelled. The CCA (solar cell, DBC, connections) is modelled for this application in order to be more generally applicable and not specific to one particular module where all the bespoke design of packaging materials would need to be introduced. The thermophysical properties and dimensions are listed in Tables 5 and 6 respectively.

The simulation ran using the Generalised Minimal RESidual method (GMRES) which is an iterative solver. The CCA configuration was meshed using the physics controlled mesh sequence as part of COMSOL. A mesh independency analysis was conducted by progressively increasing the number of elements until the temperature change was minimised; this was found to be at approximately 400,000 elements. Due to significantly lower computational time and relatively small error of 0.03% in

Table 4
Thermal boundary conditions.

No	Region	Boundary condition
1	C1MJ solar cell surface	Heat source as found from EM Eq. (10)
2	All free surfaces on top and sides	Natural convection
3	All free surfaces	Surface to ambient radiation
4	Back plate surface	Variable convective heat transfer coefficient (Table 1)
5	Ambient	Variable ambient temperature (Table 1)
6	All surfaces	Initial temperature (=25 °C)

Table 5
Materials' thermophysical properties.

Material	k (W/(mK))	Cp (J/(kgK))	ρ (kg/m^3)	ε
Germanium	60	320	5323	0.9
Copper	400	385	8700	0.05
Al_2O_3 Ceramic	30	900	3900	0.75
Silver	430	235	10,490	0.03

Table 6
Assembly's dimensions.

Layer	Thickness (mm)	Length (mm)	Width (mm)
C1MJ solar cell	0.19	10	10
Copper	0.25	24	19.5
Al_2O_3 Ceramic	0.32	25.5	21
Copper	0.25	25	20.5
Busbar	0.006	10	0.305
Contacts	0.025	10	3.5

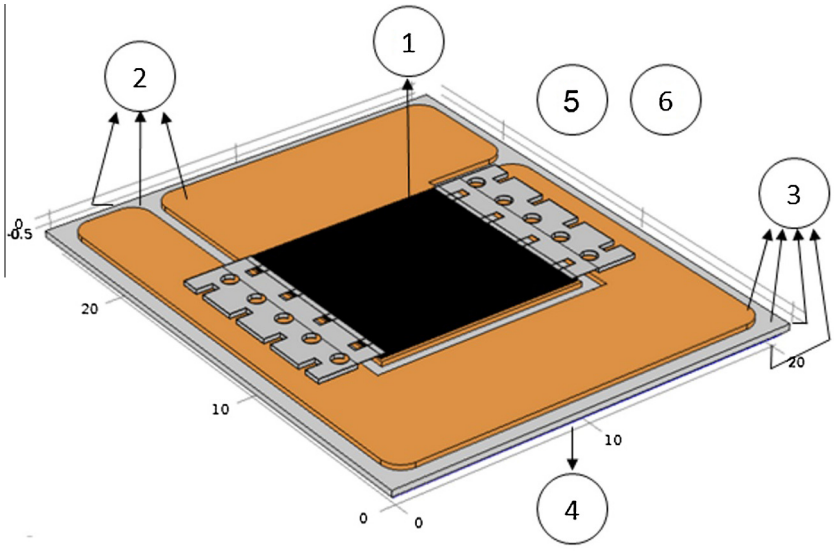

Fig. 15. Geometry and thermal boundary conditions of 3D C1MJ thermal model.

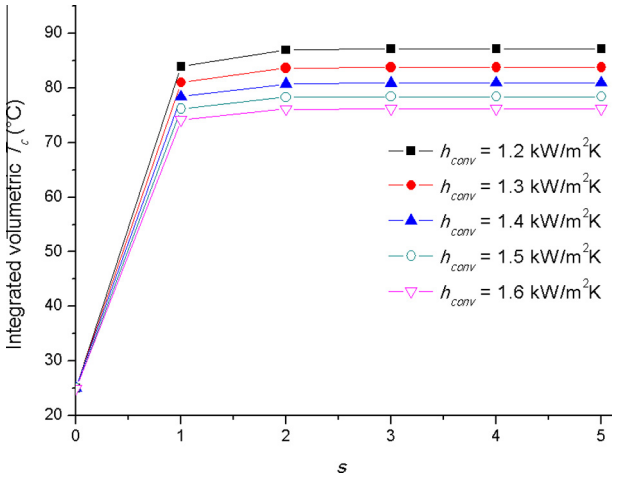

Fig. 16. Integrated volumetric solar cell temperature as a function of the cycle iteration, ambient temperature $T_{amb} = 35$ °C and AM1D.

maximum temperature, a fine mesh setting with 237,288 elements over a 435 mm^3 mesh volume was used.

The 3J C1MJ solar cell is modelled as a heat source. All the free areas at the top release heat to the environment through external natural convection and surface radiation. The back-plate's surface (copper) releases heat to the environment through surface to ambient radiation and also convection where the convective heat transfer coefficient is varied and discussed in greater detail in this section. The air temperature is also varied. For reliability purposes, all the cases up to a cell temperature of 100 °C are examined, as the cell can degrade if operated at higher temperatures for a prolonged time (Espinet-González et al., 2014).

As described in Section 3 and the flowchart in Fig. 2, the integrated model runs iteratively for an initial temperature of $T_c(s) = 25$ °C; the electrical model calculates the heat power at 25 °C and the thermal model runs for steady state. The calculated $T_c(s+1)$ from the thermal model is then imported back to the electrical model to calculate the heat power at $T_c(s+1)$. The iterations are continued until a difference lower or equal to 0.002 K is achieved. Fig. 16 shows the integrated volumetric solar cell's temperature after 6 iterations for convective heat transfer coefficients ranging from 1200 W/(m^{2}K) to 1600 W/(m^{2}K) and a constant $T_{amb} = 35$ °C. The solution is shown to converge in all cases after the 3rd iteration.

Fig. 17 shows the temperature distribution across the C1MJ solar cell for AM1D, $h_{conv} = 1600$ W/(m^{2}K) (i.e. $R_{th} = 1/(h_{conv} A) = 1.22$ K/W, area of 5.13×10^{-4} m^2) and $T_{amb} = 45$ °C. A maximum temperature of 90.33 °C is observed in the centre of the cell while the temperature of the top layer of the DBC board, which is not illuminated, is from 70 °C at the edges to 80 °C near the cell. The integrated volumetric temperature of the solar cell is 86.82 °C.

In Fig. 18, the solar cell's temperature is estimated for 1200 W/(m^{2}K) $\leqslant h_{conv} \leqslant$ 1600 W/(m^{2}K) and 25 °C $\leqslant T_{amb} \leqslant$ 45 °C. Each point in the graph represents 5 simulations/iterations as shown in Fig. 16. Ambient air temperature has a strong influence on the cell's temperature, with approximately degree directly proportion increase in temperature with air temperature. At AM1D, where the integrated direct spectral intensity is 988.8 W/m^2 and an ambient temperature of 45 °C, the C1MJ CCA can be cooled sufficiently by a convective heat transfer coefficient,

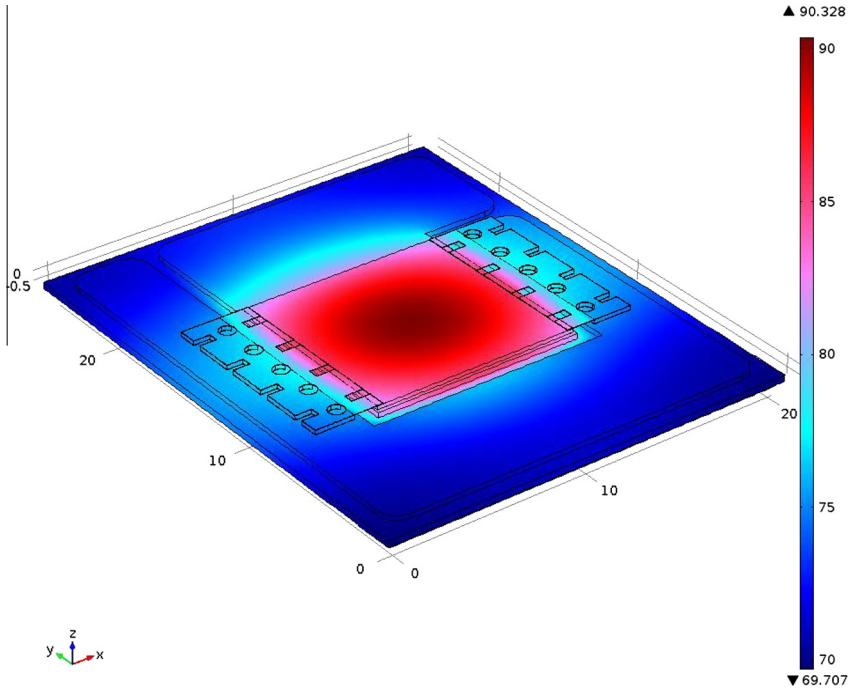

Fig. 17. Temperature distribution (°C) across the C1MJ CCA for $h_{conv} = 1.6$ kW/(m^{2}K) and $T_{amb} = 45$ °C.

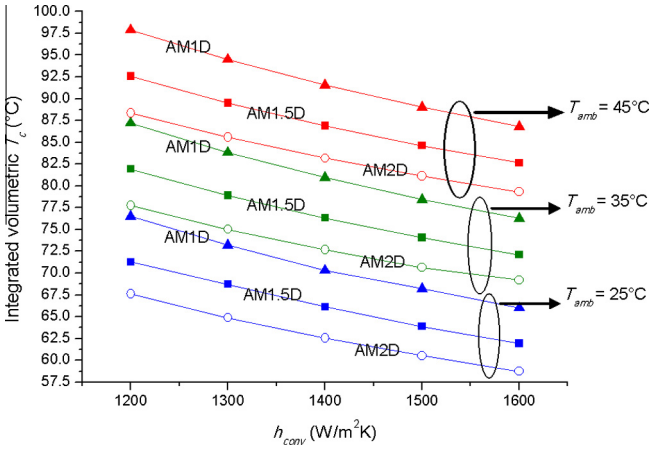

Fig. 18. Integrated volumetric solar cell temperature as a function of convective heat transfer coefficient, air mass (triangle AM1D, square AM1.5D, circle AM2D) and ambient temperature (blue 25 °C, green 35 °C, red 45 °C). (For interpretation of the references to colour in this figure legend, the reader is referred to the web version of this article.)

$h_{conv} > 1200$ W/(m^{2}K) if a maximum operation temperature at 100 °C is assumed. However, if the maximum temperature is set at 90 °C, then h_{conv} should be higher than 1400 W/(m^{2}K). For the same spectral conditions and ambient temperature of 35 °C, a heat transfer coefficient, $h_{conv} > 1200$ W/(m^{2}K) can adequately cool the solar cell's temperature well below 90 °C.

At AM1.5D conditions and ambient air temperature of 35 °C, the maximum solar cell temperature is 81.93 °C for a surface convective heat transfer coefficient of 1200 W/(m^{2}K) and as low as 72.12 °C for $h_{conv} = 1600$ W/(m^{2}K). However, under extreme conditions ($T_{amb} = 45$ °C), the maximum temperature is 92.59 °C for $h_{conv} = 1200$ W/(m^{2}K) and 82.64 °C for $h_{conv} = 1600$ W/(m^{2}K). At higher values of air mass, a higher thermal resistance is adequate and therefore, only up to AM2D are presented. It is also shown that $R_{th} \leqslant 1.4$ K/W ($h_{conv} > 1400$ W/(m^{2}K)) can be sufficient to maintain the cell below a safe operating limit without risking any long term degradation of the system. For locations with ambient temperatures lower than 40 °C, a higher heat sink thermal resistance may be acceptable.

5. Conclusions and future work

An integrated solar spectrum dependent electrical-thermal model is described for 3J solar cells under concentration followed by an application for the C1MJ CCA. While other traditional models predict the cooling requirements and thermal behaviour using constant parameters (AM1.5D or Global, $T_{amb} = 25$ °C, constant electrical efficiency) or empirical data from regression analysis, these models are not applicable to other assemblies since the geometry varies for different manufacturers. Also, since the solar spectrum is transient during the day, the AM1.5D does not offer representative results of the realistic operation of the solar cell in the field. Instead, designing the cooling or heat sinking requirements at $AM <$ AM1.5D is much preferable because the 3J solar cell is not current matched and also because the heat is higher, due to higher solar radiation intensity.

This model examines the thermal behaviour of 3J solar cells under variable air mass, ambient temperature thus electrical characteristics and therefore, it can accurately quantify the thermal power which needs to be dissipated, including the excess thermal output due to current mismatch.

It is found that CPV single cell configurations of 1 cm^2 area, can be adequately cooled passively with a heat sink thermal resistance below 1.63 K/W while for locations with extreme ambient conditions, a thermal resistance less than 1.4 K/W is needed to keep the CCA operate under 90 °C. Solar cells with lower area can withstand higher concentrations for the same thermal resistance values or higher thermal resistance at CR of 500×.

This study investigates the thermal behaviour of a solar cell assembly; however the concentrator optics are not modelled in terms of their spectral transmittance or reflectivity as a function of temperature. Increasing temperatures on refractive optics will result in a change in the refractive index of the lens due to thermal expansion; this will lead to an increase in the focal length and therefore change the overall system power generation (Hornung et al., 2012). Also, the non-uniformity of the irradiance on the surface of the solar cell has not been considered in this work; Jaus et al. (2008) considered the inhomogeneous intensity of the sun by dividing the solar cell area into different regions. Jaus et al. (2008) did not consider the spectral dependent irradiance, which is considered here. If the spectral optical efficiency as a function of temperature and the inhomogeneity of spectral irradiance are incorporated in the model, the accuracy of the model is likely to be increased further.

Acknowledgements

The support of the Engineering and Physical Sciences Research Council (EPSRC), UK and the Department of Science and Technology (DST), India is acknowledged for funding the BioCPV project (EP/J000345/1). The authors would like to thank Dr. Christian A. Gueymard for his comments on the SMARTS2 simulations.

References

Al-Amri, F., Mallick, T.K., 2013. Alleviating operating temperature of concentration solar cell by air active cooling and surface radiation. Appl. Therm. Eng. 59, 348–354.

Araki, K., Uozumi, H., Yamaguchi, M., 2002. A simple-passive cooling structure and its heat analysis for 500 X concentrator PV module. In: 29th IEEE PVSC, New Orleans, LA, USA, pp. 1568–1571.

Azurspace, 2010. CPV triple junction solar cell assembly – Type 3C40A data sheet. <http://azurspace.de/images/pdfs/CPV%20TJ%20Solar%20Cell%203C40A%2032x37mm.pdf> (accessed 08.08.14).

Azurspace, 2014. CPV triple junction solar cell assembly – Type 3C42A data sheet. <http://azurspace.com/images/products/DB_3987-00-00_3C42_AzurDesign_EFA_10x10_2014-03-27.pdf> (accessed 08.08.14).
Ben Or, A., Appelbaum, J., 2013. Estimation of multi-junction solar cell parameters. Progr. Photovolt. 21, 713–723.
Chou, T.L., Shih, Z.H., Hong, H.F., Han, C.N., Chiang, K.N., 2012. Thermal performance assessment and validation of high-concentration photovoltaic solar cell module. IEEE Trans. Comp. Packag. Manuf. Technol. 2, 578–586.
Cotal, H., Frost, J., 2010. Heat transfer modeling of concentrator multijunction solar cell assemblies using finite difference techniques. In: 35th IEEE PVSC, Honolulu, HI, USA.
Cotal, H., Sherif, R., 2006. Temperature dependence of the IV parameters from triple junction GaInP/InGaAs/Ge concentrator solar cells. In: 4th World Conference on Photovoltaic Energy Conversion, IEEE, pp. 845–848.
Dominguez, C., Anton, I., Sala, G., 2010. Multijunction solar cell model for translating I–V characteristics as a function of irradiance, spectrum, and cell temperature. Prog. Photovoltaics Res. Appl. 18, 272–284.
Espinet-González, P., Algora, C., Núñez, N., Orlando, V., Vázquez, M., Bautista, J., Araki, K., 2014. Temperature accelerated life test on commercial concentrator III–V triple-junction solar cells and reliability analysis as a function of the operating temperature. Prog. Photovoltaics Res. Appl., n/a–n/a.
Faine, P., Kurtz, S.R., Riordan, C., Olson, J.M., 1991. The influence of spectral solar irradiance variations on the performance of selected single-junction and multijunction solar-cells. Solar Cells 31, 259–278.
Fernández, E.F., Almonacid, F., Rodrigo, P., Pérez-Higueras, P., 2013. Model for the prediction of the maximum power of a high concentrator photovoltaic module. Sol. Energy 97, 12–18.
Fernández, E.F., Almonacid, F., Rodrigo, P., Pérez-Higueras, P., 2014a. Calculation of the cell temperature of a high concentrator photovoltaic (HCPV) module: a study and comparison of different methods. Sol. Energy Mater. Sol. Cells 121, 144–151.
Fernandez, E.F., Loureiro, A.J.G., Rodrigo, P., Almonacid, F., Fernandez, J.I., Higueras, P.J.P., Almonacid, G., Loureiro, A.J.G., 2013a. Calculation of cell temperature in a HCPV module using V-oc. In: Spanish Conference on Electron Devices, pp. 317–320.
Fernández, E.F., Rodrigo, P., Almonacid, F., Pérez-Higueras, P., 2014b. A method for estimating cell temperature at the maximum power point of a HCPV module under actual operating conditions. Sol. Energy Mater. Sol. Cells 124, 159–165.
Fernandez, E.F., Siefer, G., Almonacid, F., Loureiro, A.J.G., Perez-Higueras, P., 2013b. A two subcell equivalent solar cell model for III-V triple junction solar cells under spectrum and temperature variations. Sol. Energy 92, 221–229.
Gueymard, C.A., 1995. Simple model of the atmospheric radiative transfer of sunshine, version 2 (SMARTS2): algorithms description and performance assessment. Report FSEC-PF-270-95. Florida Solar Energy Center.
Gueymard, C.A., 2001. Parameterized transmittance model for direct beam and circumsolar spectral irradiance. Sol. Energy 71, 325–346.
Gueymard, C.A., Myers, D., 2010. Solar Resource for Space and Terrestrial Applications. In: Solar Cells and their Applications. John Wiley & Sons, Inc.
Gueymard, C.A., Myers, D., Emery, K., 2002. Proposed reference irradiance spectra for solar energy systems testing. Sol. Energy 73, 443–467.
Guter, W., Schone, J., Philipps, S.P., Steiner, M., Siefer, G., Wekkeli, A., Welser, E., Oliva, E., Bett, A.W., Dimroth, F., 2009. Current-matched triple-junction solar cell reaching 41.1% conversion efficiency under concentrated sunlight. Appl. Phys. Lett., 94
Helmers, H., Schachtner, M., Bett, A.W., 2013. Influence of temperature and irradiance on triple-junction solar subcells. Sol. Energy Mater. Sol. Cells 116, 144–152.
Hornung, T., Steiner, M., Nitz, P., 2012. Estimation of the influence of Fresnel lens temperature on energy generation of a concentrator photovoltaic system. Sol. Energy Mater. Sol. Cells 99, 333–338.
Incropera, F.P., DeWitt, D.P., 1996. Fundamentals of Heat and Mass Transfer. John Wiley & Sons, New York.
Jaus, J., Hue, R., Wiesenfarth, M., Peharz, G., Bett, A.W., 2008. Thermal management in a passively cooled concentrator photovoltaic module. In: 23rd European Photovoltaic Solar Energy Conference. Valencia, Spain.
Kinsey, G., 2010. High-Concentration, III–V Multijunction Solar Cells. In: Solar Cells and their Applications. John Wiley & Sons, Inc.
Kinsey, G.S., Edmondson, K.M., 2009. Spectral response and energy output of concentrator multijunction solar cells. Progr. Photovolt. 17, 279–288.
Kinsey, G.S., Hebert, P., Barbour, K.E., Krut, D.D., Cotal, H.L., Sherif, R.A., 2008. Concentrator multijunction solar cell characteristics under variable intensity and temperature. Progr. Photovolt. 16, 503–508.
Kribus, A., Kaftori, D., Mittelman, G., Hirshfeld, A., Flitsanov, Y., Dayan, A., 2006. A miniature concentrating photovoltaic and thermal system. Energy Convers. Manage. 47, 3582–3590.
Kuo, A.Y., Lin, B., Huang, C.C., Chen, J., Chiang, P.K., Shao, S., Wu, R., Lin, I., 2009. A modular solar engine with solar cell, heat pipe, and heat sink in an integrated package for high concentrating photovoltaic. In: 34th IEEE PVSC, Philadelphia, PA, USA, pp. 166–169.
Min, C., Nuofu, C., Xiaoli, Y., Yu, W., Yiming, B., Xingwang, Z., 2009. Thermal analysis and test for single concentrator solar cells. J. Semiconduct., 30
Mudawar, I., 2001. Assessment of high-heat-flux thermal management schemes. IEEE Trans. Comp. Packag. Technol. 24, 122–141.
Natarajan, S.K., Mallick, T.K., Katz, M., Weingaertner, S., 2011. Numerical investigations of solar cell temperature for photovoltaic concentrator system with and without passive cooling arrangements. Int. J. Therm. Sci. 50, 2514–2521.
Nishioka, K., Takamoto, T., Agui, T., Kaneiwa, M., Uraoka, Y., Fuyuki, T., 2005. Evaluation of temperature characteristics of high-efficiency InGaP/InGaAs/Ge triple-junction solar cells under concentration. Sol. Energy Mater. Sol. Cells 85, 429–436.
Nishioka, K., Takamoto, T., Agui, T., Kaneiwa, M., Uraoka, Y., Fuyuki, T., 2006. Annual output estimation of concentrator photovoltaic systems using high-efficiency InGaP/InGaAs/Ge triple-junction solar cells based on experimental solar cell's characteristics and field-test meteorological data. Sol. Energy Mater. Sol. Cells 90, 57–67.
NREL, 2015. National Center for Photovoltaics. Best research-cell efficiencies chart. <http://www.nrel.gov/ncpv/images/efficiency_chart.jpg> (accessed 11.03.15).
Rabady, R.I., 2014. Optimized multi-junction photovoltaic solar cells for terrestrial applications. Sol. Energy 106, 72–81.
Rodrigo, P., Fernández, E., Almonacid, F., Pérez-Higueras, P., 2013. Models for the electrical characterization of high concentration photovoltaic cells and modules: a review. Renew. Sustain. Energy Rev. 26, 752–760.
Rodrigo, P., Fernández, E.F., Almonacid, F., Pérez-Higueras, P.J., 2014. Review of methods for the calculation of cell temperature in high concentration photovoltaic modules for electrical characterization. Renew. Sustain. Energy Rev. 38, 478–488.
Royne, A., Dey, C.J., 2007. Design of a jet impingement cooling device for densely packed PV cells under high concentration. Sol. Energy 81, 1014–1024.
Royne, A., Dey, C.J., Mills, D.R., 2005. Cooling of photovoltaic cells under concentrated illumination: a critical review. Sol. Energy Mater. Sol. Cells 86, 451–483.
Segev, G., Mittelman, G., Kribus, A., 2012. Equivalent circuit models for triple-junction concentrator solar cells. Sol. Energy Mater. Sol. Cells 98, 57–65.
Siefer, G., Bett, A.W., 2014. Analysis of temperature coefficients for III–V multi-junction concentrator cells. Prog. Photovoltaics Res. Appl. 22, 515–524.
Spectrolab, 2009a. Application Note 0902 – Analytical model for C1MJ and C3MJ CDO-100 Solar Cells and CCAs. Spectrolab, Sylmar, CA
Spectrolab, 2009b. C1MJ Concentrator Solar Cell Assembly Data Sheet (prototype product). <http://www.spectrolab.com/DataSheets/PV/CPV/C1MJ%2009%2018%2009.pdf> (accessed 10.06.14).

Steiner, M., Siefer, G., Bosch, A., Hornung, T., Bett, A.W., 2012. Realistic Power Output Modeling of CPV Modules. In: CPV-8, Toledo, Spain, pp. 309–312.

Theristis, M., O'Donovan, T.S., 2014. An integrated thermal electrical model for single cell photovoltaic receivers under concentration. In: 15th International Heat Transfer Conference (IHTC-15), Kyoto, Japan, n/a–n/a.

Varshni, Y., 1967. Temperature dependence of the energy gap in semiconductors. Physica 34, 149–154.

Verlinden, P.J., Lewandowski, A., Bingham, C., Kinsey, G.S., Sherif, R.A., Lasich, J.B., 2006. Performance and reliability of multijunction III–V modules for concentrator dish and central receiver applications. In: 4th World Conference on Photovoltaic Energy Conversion, Hawaii, IEEE, pp. 592–597.

Wang, Y.N., Lin, T.T., Leong, J.C., Hsu, Y.T., Yeh, C.P., Lee, P.H., Tsai, C.H., 2013. Numerical investigation of high-concentration photovoltaic module heat dissipation. Renewable Energy 50, 20–26.

Yandt, M.D., Wheeldon, J.F., Cook, J., Beal, R., Walker, A.W., Theriault, O., Schriemer, H., Hall, T.J., Hinzer, K., 2012. Estimating cell temperature in a concentrating photovoltaic system. In: CPV-8, Toledo, Spain, pp. 172–175.

Ye, Z.B., Li, Q.F., Zhu, Q.Z., Pan, W.G., 2009. The cooling technology of solar cells under concentrated system. In: 6th IEEE IPEMC, Wuhan, China, pp. 1252–1256.

Zhu, L., Boehm, R.F., Wang, Y.P., Halford, C., Sun, Y., 2011. Water immersion cooling of PV cells in a high concentration system. Sol. Energy Mater. Sol. Cells 95, 538–545.